ACS APPLIED MATERIALS & INTERFACES

www.acsami.org
Research Article

Heating Efficiency of Different Magnetotactic Bacterial Species: Influence of Magnetosome Morphology and Chain Arrangement

Danny Villanueva, Alicia G. Gubieda, Lucía Gandarias, Ana Abad Díaz de Cerio, Iñaki Orue, José Angel García, David de Cos, Javier Alonso, and M. Luisa Fdez-Gubieda*

Cite This: ACS Appl. Mater. Interfaces 2024, 16, 67216−67224

ABSTRACT: Magnetotactic bacteria have been proposed as ideal biological nanorobots due to the presence of an intracellular chain of magnetic nanoparticles (MNPs), which allows them to be guided and controlled by external magnetic fields and provides them with theragnostic capabilities intrinsic to magnetic nanoparticles, such as magnetic hyperthermia for cancer treatment. Here, we study three different bacterial species, *Magnetospirillum gryphiswaldense* (MSR-1), *Magnetospirillum magneticum* (AMB-1), and *Magnetovibrio blakemorei* (MV-1), which synthesize magnetite nanoparticles with different morphologies and chain arrangements. We analyzed the impact of these parameters on the effective magnetic anisotropy, K_{eff}, and the heating capacity or Specific Absorption Rate, SAR, under alternating magnetic fields. SAR values have been obtained from the area of experimental AC hysteresis loops, while K_{eff} has been determined from simulations of AC hysteresis loops using a dynamic Stoner−Wohlfarth model. The results demonstrate a clear relationship between the effective magnetic anisotropy and the heating efficiency of bacteria. As the K_{eff} value increases, the saturated SAR values are higher; however, the threshold magnetic field required to observe a SAR response simultaneously increases. This factor is crucial to choose a bacterial species as the optimal hyperthermia agent.

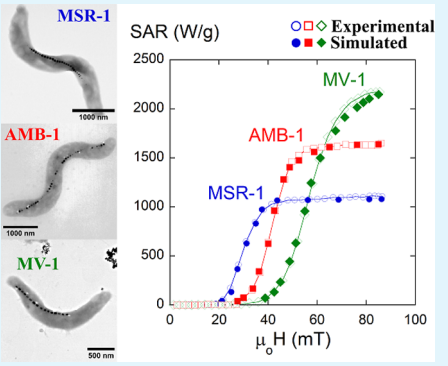

KEYWORDS: *specific absorption rate, magnetic anisotropy, magnetosome morphology, Stoner−Wohlfarth model, magnetotactic bacteria, Magnetospirillum gryphiswaldense MSR-1, Magnetospirillum magneticum AMB-1, Magnetovibrio blakemorei MV-1*

INTRODUCTION

Cancer remains one of the leading causes of death worldwide. In 2020, 19.3 million new cancer cases and approximately 10 million cancer-related deaths were reported worldwide.[1] This figure highlights the urgent need for innovative and more efficient treatment approaches to complement existing ones. Novel strategies must address inherent limitations of standard treatments, including nonselective cytotoxicity and nonspecific targeting. In recent decades, various entities, such as magnetic nanoparticles (MNPs),[2,3] bacteria,[4−7] and viruses,[8−10] have been proposed as potential nanorobots to treat tumors. MNPs offer a significant advantage as magnetic hyperthermia therapy agents: MNPs can be injected into the tumor area, and upon application of an alternating magnetic field, they undergo a hysteresis loop, dissipating energy and raising the tumor's temperature.[11] This process induces apoptosis in cancer cells while sparing healthy ones. The use of MNPs in hyperthermia has been explored extensively in several key reviews, which discuss the optimization of magnetic nanoparticles for hyperthermia applications and their clinical potential.[12,13] However, despite these extensive studies and numerous efforts to improve their magnetic and heating properties,[14−16] MNPs exhibit several limitations, such as the absence of self-propelling mobility, low environmental responsiveness, and limited targeting efficiency. Bacterial therapy, on the other hand, capitalizes on motility, which enables bacteria to actively penetrate deep into the tumor tissue, thereby stimulating the immune system.[4]

Magnetotactic bacteria (MTB) have emerged as promising biological nanorobots, as they combine the advantages of MNPs and bacterial therapy.[17−20] MTB are motile aquatic microorganisms capable of aligning along the Earth's magnetic field due to intracellular magnetic nanoparticles, called magnetosomes, which they synthesize and arrange into chains along the cell's longitudinal axis.[21,22] It must be noted that the composition, morphology, and size of magnetosomes vary among bacterial species, indicating strict genetic control over their formation.[23−26] The magnetic response and heating capacity of each bacterial species depend on parameters such as the magnetic anisotropy of the magnetosome, determined mainly by the competition between magneto-crystalline and

Received: August 5, 2024
Revised: November 4, 2024
Accepted: November 7, 2024
Published: November 26, 2024

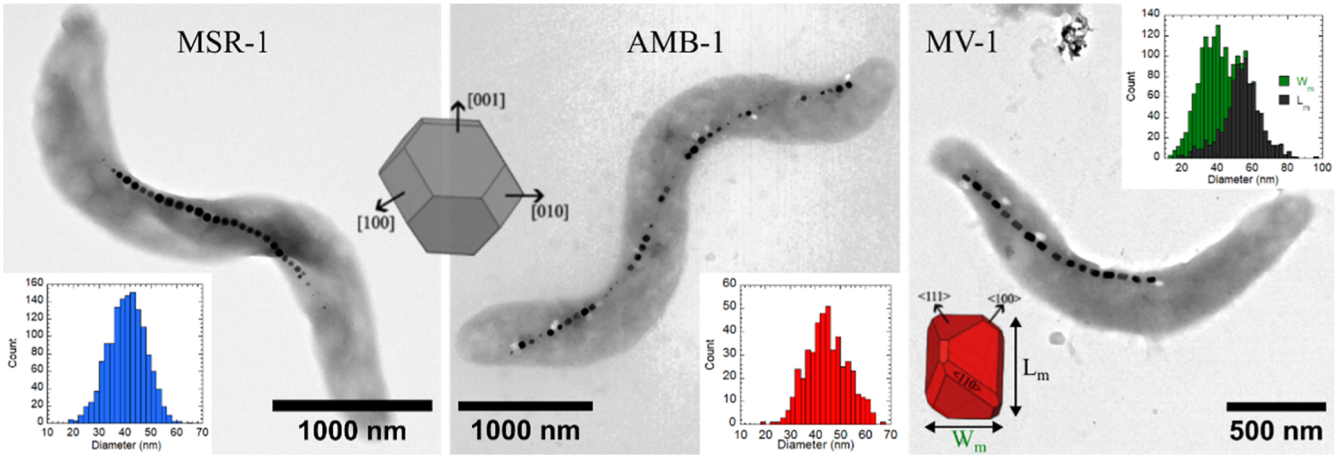

Figure 1. TEM images of *Magnetospirillum gryphiswaldense* (MSR-1), *Magnetospirillum magneticum* (AMB-1), and *Magnetovibrio blakemorei* (MV-1) with a schematic representation of the magnetosome morphology synthesized by each species: distorted cuboctahedral for MSR-1 and AMB-1, and truncated hexa-octahedral for MV-1. In the inset, a histogram with the mean diameter distribution of magnetosomes for MSR-1 and AMB-1 and the width (W) and length (L) distribution of magnetosomes for MV-1.

shape anisotropies, and the assembly of magnetosomes into chain structures that determines the dipolar interaction.[27−29]

One of the initial studies on the heating efficiency of whole magnetotactic bacteria (MTB) was conducted by Alphandery et al. in 2011[30] using the *Magnetospirillum magneticum* (AMB-1) species. In this study, the authors compared the heating efficiency of individual magnetosomes, magnetosome chains extracted from MTB, and the whole MTB. They demonstrated that whole inactive MTB in a gel could generate heat with a SAR of 125 W/g_{Fe} (90 W/$g_{Fe_3O_4}$) at 40 mT and 183 kHz, although this heating efficiency was lower compared to that of extracted magnetosome chains and individual magnetosomes. More recently, Gandia et al.[31] investigated the heating efficiency of *Magnetospirillum gryphiswaldense* (MSR-1) and compared the results with those obtained from isolated magnetosomes, both dispersed in water, finding that the heating efficiency of bacteria doubles that of the isolated magnetosomes.

In this work, we carried out a comparative study of the heating efficiency of three different bacterial species: *M. gryphiswaldense* (MSR-1), *M. magneticum* (AMB-1), and *Magnetovibrio blakemorei* (MV-1). Each species synthesizes magnetosomes of distinct morphologies and chain arrangements, and therefore different shape anisotropy and dipolar interactions are expected. However, all magnetosomes share the same magnetite composition, thereby maintaining constant magneto-crystalline anisotropy.

The bibliography provides a thorough description of the morphology of the magnetosomes synthesized by each of the studied species.[25,26,32,33] MSR-1 and AMB-1 bacteria exhibit a spirillum morphology, with their magnetosomes shaped as cuboctahedra of 40−45 nm mean diameter.[34−36] The key difference between both species lies in the arrangement of their magnetosomes within their chain: MSR-1 features a continuous chain at midcell, whereas AMB-1 displays a fragmented chain spanning the whole cell length.[33,37] In contrast, MV-1 bacteria exhibit a vibrio to spirillum shape and synthesize elongated magnetosomes with truncated hexa-octahedral morphology, with a mean size of around 35 × 35 × 53 nm^3.[32,38,39]

In the present work, we have observed the main morphological characteristics of these bacteria by transmission electron microscopy (TEM). The heating efficiency or specific absorption rate, SAR, has been evaluated at room temperature using an AC magnetometer. In these measurements, SAR values are obtained from the area of the AC hysteresis loops under an applied alternating magnetic field of frequency f = 132 kHz. A dynamic Stoner−Wohlfarth model has been employed to simulate the AC hysteresis loops. This has allowed the determination of the effective uniaxial anisotropy, K_{eff}, which defines the magnetic behavior and therefore the heating capacity of each species. The obtained K_{eff} values are 11 kJ/m^3 for MSR-1, 18 kJ/m^3 for AMB-1, and 28 kJ/m^3 for MV-1. The magnetic anisotropy determines the maximum heating efficiency value that can be reached for each species: SAR_{sat}/f = 8, 12, 16.4 W g^{-1} kHz^{-1} for MSR-1, AMB-1 and MV-1, respectively. Furthermore, it defines the minimum magnetic field amplitude that must be applied to attain those SAR values.

MATERIALS AND METHODS

Magnetotactic Bacteria Culture. The *M. gryphiswaldense* strain MSR-1 (DSMZ: DSM 6361) and *M. magneticum* strain AMB-1 (ATCC: 700264) cells were cultured at 28 °C in flask standard medium (FSM): 10 mM HEPES, 735 μM KH_2PO_4, 600 μM of $MgSO_4{\cdot}7H_2O$, 4 mM of $NaNO_3$, 0.01% (wt/vol) of yeast extract, 0.3% (wt/vol) of soybean peptone, 0.3% (wt/vol) of sodium pyruvate and 100 μM of Fe (III)-citrate. Both were cultured without shaking in 100 mL bottles with 80 mL of culture media to get a low oxygen concentration. MSR-1 bacteria were collected after 48 h to ensure the presence of well-formed magnetosome chains. AMB-1 bacteria were collected after 96 h of incubation.

The *Magnetovibrio blakemorei* strain MV-1 (DSMZ: DSM 18854) was cultured under anaerobic conditions at 30 °C in a medium containing per liter of artificial seawater (ASW): 0.4% (wt/vol) of sodium succinate × $6H_2O$, 0.08% (wt/vol) of sodium acetate, 0.1% (wt/vol) casamino acids (BD Bacto), 18.7 mM NH_4Cl, 5 mL Wolfe's mineral solution and 50 μL of 1%(w/v) resazurine. After autoclaving, 0.5 mL BME Vitamins 100× solution (Sigma-Aldrich, B6891), 1.8 mL of PO_4 buffer (0.5 M), 0.3 mL of $FeCl_2$ (10 mM) and 10 mL of freshly made cysteine solution (0.25 M) were added to the media and the pH was adjusted to 7. The media was then distributed into sterile Hungate tubes and fluxed for 20 min with N_2O. The bacteria were collected after 144 h of incubation.

In all three cases, bacteria were harvested by centrifugation at 16,000 *g* for 10 min at 4 °C, fixed with 2% glutaraldehyde and washed

https://doi.org/10.1021/acsami.4c13152
ACS Appl. Mater. Interfaces 2024, 16, 67216−67224

Table 1. Average Number of Magnetosomes per Cell (N_m), Length (L_m) and Width (W_m) of Magnetosome, Mean Diameter $(W_m + L_m)/2$, Shape Factor (W_m/L_m), Magnetosome Chain Length (L_{mc}) and Cell Length (L_{cell}).

bacterial species	N_m	W_m (nm)	L_m (nm)	$(W_m + L_m)/2$ (nm)	W_m/L_m	L_{mc} (nm)	L_{cell} (nm)
MSR-1	25(8)	39(7)	42(7)	41(7)	0.92(5)	1500(500)	4000(600)
AMB-1	31(9)	42(9)	47(8)	45(8)	0.89(6)	3000(900)	4300(700)
MV-1	23(10)	36(11)	54(8)		0.7(1)	1700(600)	3100(700)

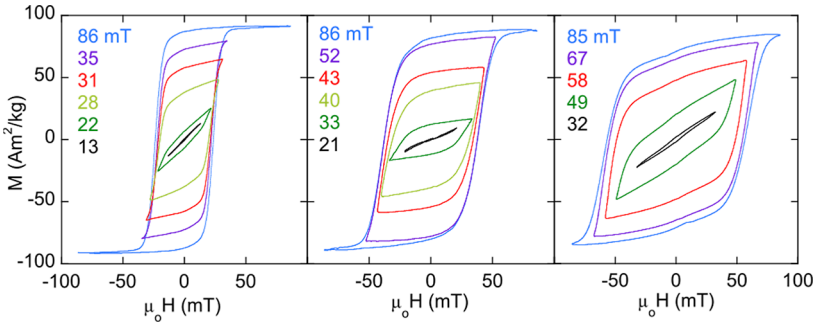

Figure 2. AC hysteresis loops measured at 132 kHz for *Magnetospirillum gryphiswaldense* (MSR-1), *Magnetospirillum magneticum* (AMB-1), and *Magnetovibrio blakemorei* (MV-1) bacteria dispersed in water. The legend shows the maximum amplitude of the applied AC magnetic field.

three times using PBS. Cultured bacteria were counted under the microscope with acridine orange staining, and final concentration up to ~10^{11} cells/mL was achieved by adjusting the volume of bacteria culture employed and the volume of Milli-Q water concentrated in.

Transmission Electron Microscopy. Transmission electron microscopy (TEM) was performed on unstained cells adsorbed onto 300 mesh carbon-coated copper grids. TEM images were obtained with a JEOL JEM-1400 Plus electron microscope at an accelerating voltage of 120 kV.

The crystal sizes were determined by measuring the major (length, L) and minor (width, W) axes of the best-fitting ellipse of the TEM images. The mean diameter was defined as $(L + W)/2$, and the shape factor as W/L. The bacteria length requires first obtaining the central curve that connects the two opposite ends of the bacteria through a skeletonisation process.[40] By measuring the length of the central curve, the length of the bacterium was obtained. On the other hand, the chain of magnetosomes was calculated by measuring the length of the curve passing through the centroid of each magnetosome.

Magnetic Hyperthermia. Magnetic hyperthermia studies have been performed using a homemade AC magnetometry setup.[41] The magnetic field amplitude ranged between 0 and 90 mT, with a frequency of 132 kHz. For these measurements, we prepared suspensions of bacteria in distilled water with a cell concentration of ~10^{11} cell/ml for MSR-1 and MV-1 and ~0.5×10^{11} cell/ml for AMB-1. The volume of the sample vial was 100 μL.

The magnetite concentration of all studied samples was determined through the DC hysteresis loops by using a vibrating sample magnetometer (VSM) with a magnetic field up to 1 T. The total magnetite concentrations were 0.28, 0.11, and 0.38 mg Fe_3O_4 mL^{-1} for MSR-1, AMB-1 and MV-1 bacteria, respectively.

EXPERIMENTAL RESULTS

Transmission electron microscopy (TEM) was employed for the morphological characterization of the magnetosomes and magnetosome chain of each species. Figure 1 illustrates the primary characteristics of the three species under study. Both MSR-1 and AMB-1 bacteria exhibit a spirillum morphology, with their magnetosomes having a cuboctahedral shape[33,35−37] and a mean diameter of ~40−45 nm, while MV-1 bacteria display a vibrio to spirillum morphology and produce elongated magnetosomes with a truncated hexa-octahedral morphology,[32,38,39] as expected. The main difference between MSR-1 and AMB-1 lies in the arrangement of their magnetosomes within the chain: MSR-1 exhibits a complete chain, whereas AMB-1 species display a fragmented one.

From the analysis of the TEM images we have determined the average number of magnetosomes per cell (N_m), length (L_m) and width (W_m) of magnetosome, the mean diameter $(W_m + L_m)/2$ and the shape factor (W_m/L_m). We have also determined the length of the magnetosome chain (L_{mc}) and the cell (L_{cell}). All these data are presented in Table 1 with the standard deviations shown in parentheses. The histograms are shown in the Supporting Information, Figures S1−S5.

The average number of magnetosomes per chain is similar for the three different bacterial species, ranging from 23(10) to 31(9). Crystal size was determined by measuring the width (W_m) and length (L_m) of the best-fitting ellipse of the magnetosome TEM images. The mean diameter was calculated as $(W_m + L_m)/2$ for MSR-1, 41(7) nm, and AMB-1, 45(8) nm.

On the other hand, the magnetosome shape factors (W_m/L_m) found for the different bacterial species are very similar to those reported by other authors: 0.92(5) for MSR-1,[42] 0.89(6) for AMB-1[43,44] and 0.7(1) for MV-1.[45] This parameter is a key issue for understanding the effective magnetic anisotropy since it defines the shape anisotropy of the magnetosome. Finally, regarding the morphology of the bacteria and the magnetosome chain, the most remarkable difference between them is that in MSR-1 and MV-1 the chain is located in the center of the cell, whereas in AMB-1 the magnetosome chain is fragmented and spans the entire cell, resulting in a longer chain.

The SAR response of each species was determined by measuring the hysteresis loops using an AC magnetometer, since the area of the AC hysteresis loop is proportional to the magnetic energy losses arising from Brownian and Néel relaxation contributions.[46,47] The measured hysteresis loops for MSR-1, AMB-1 and MV-1 bacteria are presented in Figure 2. Several noteworthy observations can be made regarding the evolution of these AC loops. All species exhibit similar behavior: as the applied magnetic field increases, the AC loops change from an anhysteretic shape at very low magnetic fields to a lancet shape at medium amplitudes, and finally to a rectangular one at high magnetic fields.

The appearance of rectangular hysteresis loops clearly indicates that the whole bacterium orientates in the direction of the applied magnetic field, giving rise to the typical Stoner−Wohlfarth hysteresis loop for an uniaxial system in which the easy axis is parallel to the applied magnetic field. This is the optimal configuration to maximize the area of the hysteresis loop and therefore achieve the highest heating efficiency.[48]

The heating efficiency is quantified by the specific absorption rate value, SAR, given by[47]

https://doi.org/10.1021/acsami.4c13152
ACS Appl. Mater. Interfaces 2024, 16, 67216−67224

$$\text{SAR (W/g)} = \frac{f}{c} \cdot \oint \mu_0 M_t \mathrm{d}H_t. \quad (1)$$

Here, M_t is the instantaneous magnetization at time t; H_t represents the amplitude of the alternating magnetic field of frequency f at time t; and c is the weight concentration of magnetosomes in the medium.

Figure 3 displays the evolution of the SAR values as a function of the applied magnetic field amplitude, $\mu_0 H$, for MSR-1, AMB-1, and

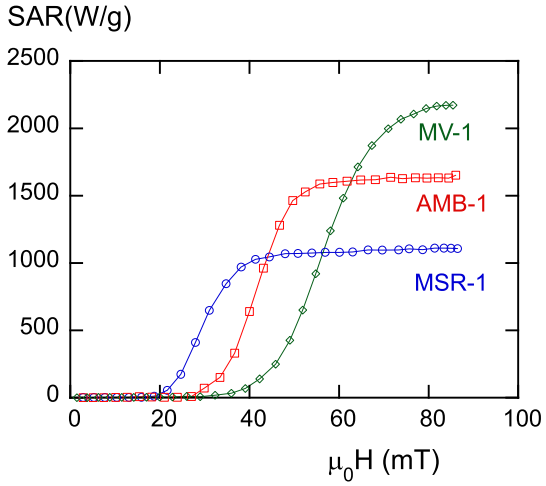

Figure 3. Specific absorption rate, SAR, measured at 132 kHz as a function of magnetic field amplitude for *Magnetospirillum gryphiswaldense* (MSR-1), *Magnetospirillum magneticum* (AMB-1), and *Magnetovibrio blakemorei* (MV-1) bacteria dispersed in water.

MV-1 dispersed in water. It is noteworthy that the qualitative SAR response to the magnetic field amplitude is very similar in all species. First, at low magnetic fields, SAR values are negligible; then, once a species dependent threshold field is reached (see $\mu_0 H_{th}$ values in Table 2), SAR shows a rapid increase. Finally, above a species dependent magnetic field (see $\mu_0 H_{sat}$ values in Table 2), SAR reaches saturation. To this respect, previous studies have demonstrated that tuning the particle size and magnetic anisotropy of iron oxide MNPs can effectively modulate the threshold field and enhance the SAR values.[49,50]

Table 2. $\mu_0 H_{th}$: Threshold Field to Observe a SAR Response; $\mu_0 H_{sat}$: Minimum Value of Applied Magnetic Field to Reach the Saturation Value of Specific Absorption Rate; SAR_{sat}/f: Saturation Value of Specific Absorption Rate Normalized by the Frequency; K_{eff} (σ_K): Effective Uniaxial Anisotropy and the Standard Deviation Used for the Simulations

bacterial species	$\mu_0 H_{th}$ (mT)	$\mu_0 H_{sat}$ (mT)	SAR_{sat}/f (Wg^{-1} kHz^{-1})	K_{eff} (σ_K) (kJ m^{-3})
MSR-1	21	41	8	11 (2)
AMB-1	29	55	12	18 (4)
MV-1	36	83	16,4	28 (4)

These findings clearly demonstrate that the morphology of the magnetosomes and their chain arrangement significantly influence the heating efficiency of the bacteria, with each species showing their optimal heating results at different working field amplitudes. In addition, these results showcase that bacteria suspended in water exhibit significantly higher SAR values compared to immobilized bacteria or isolated magnetosomes, as previously observed in other studies.[20,31]

DYNAMIC STONER-WOHLFARTH SIMULATIONS

The bacteria dispersed in water behave as highly anisotropic magnetic dipole system, due to the presence of their magnetosome chain and the capability to orientate themselves with magnetic field. In this system, the intrinsic magnetocrystalline cubic anisotropy, characteristic of magnetite, plays a minor role in the definition of the hysteresis loops.[51] To analyze them, we conducted simulations using a dynamic Stoner−Wohlfarth model for an uniaxial anisotropy system. The uniaxial system is defined by an effective anisotropy, K_{eff}, arising from the shape anisotropy and dipolar interactions between the magnetosomes in the chain.

A comprehensive description of this model can be found in ref 52. In summary, we treated the magnetosome chain as a collection of independent single-domain particles, thermally stable at room temperature. The energy density of a magnetic single domain, $E(\theta, \phi)$ depends on the orientation of the magnetization, $\hat{u}_m$, with θ and ϕ being the polar and azimuthal angles, in spherical coordinates. For an uniaxial anisotropy system, with easy axis, $\hat{u}_{uni}$, the energy density $E(\theta, \phi)$ in the presence of an external AC magnetic field, $\vec{H} = H_0 \sin(\omega t)\hat{u}_H$, is given by

$$E(\theta, \phi) = K_{eff}(1 - (\hat{u}_{uni} \cdot \hat{u}_m)^2) - \mu_0 M_s H(\hat{u}_H \cdot \hat{u}_m) \quad (2)$$

The determination of M_H (magnetization projection over H), for a given function $E(\theta, \phi)$, is carried out using a simple dynamical approach to consider the thermal activation. In this approach, the magnetization of the single domain can switch between available energy minima states at a rate determined by the well-known Arrhenius law,[53]

$$\nu_{ij}(t) = \nu_0 e^{-\Delta E_{i,j} V / k_B T} \quad (3)$$

where ν_0 is the attempt frequency, which we have considered as $\nu_0 \approx 10^9$ Hz.[52,54] The term $\Delta E_{i,j} V$ represents the energy barriers between such minima, with V being the particle volume, which can be calculated from the field-dependent energy landscape. Finally, $k_B T$ is the thermal energy. All the experiments in this work have been performed at room temperature.

The magnetization, M_H, is given by

$$M_H(t) = M \sum_i p_i(H) \hat{u}_i(H) \cdot \hat{u}_H(t) \quad (4)$$

where $p_i(H)$ are the probabilities of finding the magnetization in state i, and $\hat{u}_i(t)$ are the director vectors that define the positions of the energy minima, which depend on the external field $\vec{H}(t) = H_0 \sin(\omega t)\hat{u}_H$.

In this way, probabilities $p_i(H)$ can be calculated by numerically solving ordinary differential equations

$$\frac{\partial p_i}{\partial t} = \sum_{j \neq i} \nu_{ji} p_j - \left(\sum_{j \neq i} \nu_{ij} \right) p_i \quad (5)$$

This equation illustrates that the change in population i is determined by the balance between incoming jumps (first term) and outgoing jumps (second term) to or from the other minimum states. This balance ensures the conservation of magnetization $\sum p_i = 1$.

For low magnetic fields, the bacteria are considered to be randomly dispersed in water. The application of an external magnetic field will result in the bacteria orienting themselves in

https://doi.org/10.1021/acsami.4c13152
ACS Appl. Mater. Interfaces 2024, 16, 67216−67224

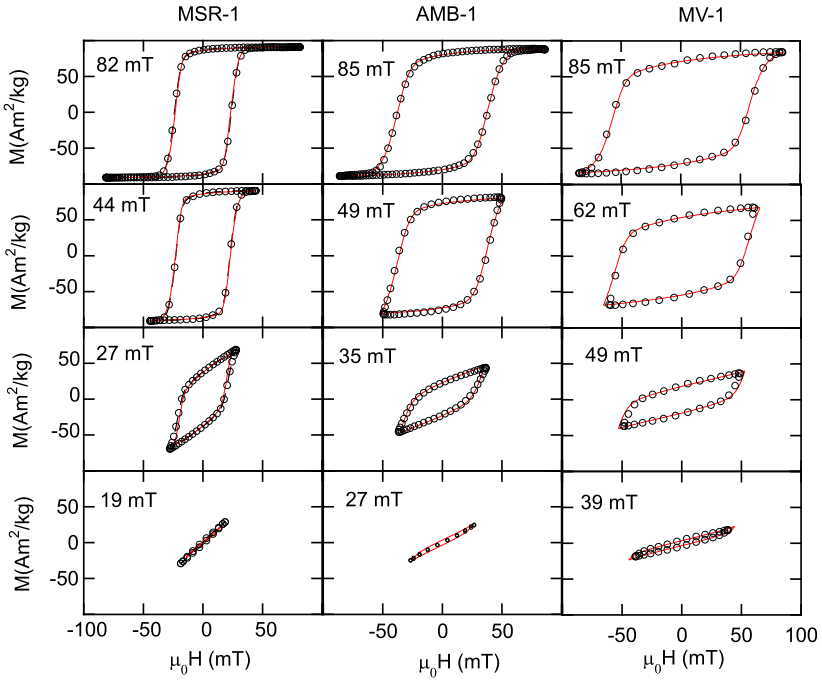

Figure 4. Experimental (o) and simulated (—) AC hysteresis loops measured at 132 kHz at different amplitudes of the magnetic field for *Magnetospirillum gryphiswaldense* (MSR-1), *Magnetospirillum magneticum* (AMB-1), and *Magnetovibrio blakemorei* (MV-1) bacteria dispersed in water.

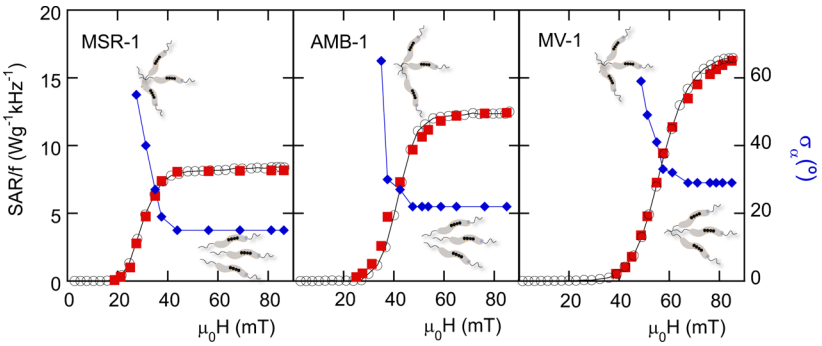

Figure 5. Experimental (o) and simulated (□) specific absorption rate normalized by the frequency f = 132 kHz, SAR/f, for *Magnetospirillum gryphiswaldense* (MSR-1), *Magnetospirillum magneticum* (AMB-1), and *Magnetovibrio blakemorei* (MV-1) bacteria dispersed in water. (◊) Standard angular deviation, σ_α, of bacteria with respect to the direction of the applied magnetic field. A schematic representation of the orientation of bacteria is included.

the direction of the field. Even when working with magnetic nanoparticles, it has been observed that the application of an alternating magnetic field can result in the formation of chains of nanoparticles, which is dependent on the amplitude of the magnetic field.[55−57] To account for this phenomenon, a Gaussian angular distribution, $P(\alpha)$, has been introduced into the magnetization expression, where the standard angular deviation, σ_α, will model the angular deviation of bacteria with the direction of the applied magnetic field. Furthermore, to incorporate a dispersion of the anisotropy constant we have also included a Gaussian distribution for the uniaxial anisotropy constant, $P(K)$, which accounts for variability in the shape of the magnetosomes. Finally, the magnetization is given by

$$M = \int_0^{\pi/2} P(\alpha)\mathrm{d}\alpha \int P(K)\mathrm{d}K \int_0^{\pi} M_H \, d\lambda \qquad (6)$$

Figure 4 presents a comparison between the simulations and the experimental AC hysteresis loops (see Supporting Information for more detail). There is an excellent agreement between both data, experimental and simulations, for an effective anisotropy value, K_{eff}, characteristic of each bacterial species and given in Table 2.

It should be noted that the simulations were conducted under the assumption that for each magnetic field amplitude, bacteria dispersed in water would have a different orientation with respect to the applied magnetic field direction. For magnetic fields below a threshold value, $\mu_0 H < \mu_0 H_{th}$, bacteria are assumed to be randomly distributed. For magnetic fields higher than the threshold field, $\mu_0 H > \mu_0 H_{th}$, bacteria begin to orientate themselves in the direction of the applied magnetic field. As the amplitude of the magnetic field is increased, the orientation of bacteria is higher and as a consequence the standard angular deviation values, σ_α, decrease. At a certain magnetic field, $\mu_0 H = \mu_0 H_{sat}$, the field at which the SAR/f

https://doi.org/10.1021/acsami.4c13152
ACS Appl. Mater. Interfaces 2024, 16, 67216−67224

reaches saturation, the bacteria exhibit near-complete orientation with the direction of the applied magnetic field, thus σ_α reaching the minimum value. The σ_α values are shown in Figure 5.

Finally, the SAR/f values are obtained from the area of the simulated hysteresis loops. These are presented in Figure 5 together with the experimental data, which demonstrate a perfect match.

DISCUSSION

The magnetotactic bacteria, due to the presence of the magnetosome chain, exhibit an effective uniaxial magnetic anisotropy, K_{eff}, that can be readily simulated with a dynamical Stoner−Wohlfarth model. This uniaxial anisotropy arises from the shape anisotropy of the magnetosomes and the dipolar interaction between the magnetosomes in the chain. The K_{eff} values utilized in the simulation are presented in Table 2. For the MSR-1 and AMB-1 species, the effective anisotropy values are 11(2) and 18(4) kJ m^{-3}, respectively. The values obtained are highly comparable to those derived from the analysis of DC hysteresis loops, 12(1) and 16(4) kJ m^{-3} for MSR-1 and AMB-1 respectively.[37,58] Both bacterial species synthesize magnetite with cuboctahedral morphology. This morphology results in a cubic anisotropy, but previous results of electron cryotomography have demonstrated that the magnetosomes produced by MSR-1 exhibit a distinct shape distortion:[35] 10% distortion on the <111> direction and 7,5% on the <100> direction, resulting in a uniaxial shape anisotropy of 7 kJ/m^3. This is consistent with the shape factor found from the TEM analysis for MSR-1, W_m/L_m = 0.92(5). In addition, the higher value of the effective magnetic anisotropy found for AMB-1 is consistent with the lower shape factor for AMB-1, W_m/L_m = 0.89(6). In contrast, the MV-1 species presents an effective magnetic anisotropy constant of 28(4) kJ m^{-3}. This value is notably higher, reflecting the fact that this species synthesizes elongated magnetosomes, with a shape factor of 0.7(1), which give rise to a strong uniaxial shape magnetic anisotropy of 22 kJ m^{-3} as determined by finite element simulations.[38]

Finally, it should be noted that the different effective magnetic anisotropy arises from both variations in the distortion of the magnetosomes shape and changes in the dipolar interactions due to different magnetosome arrangements.

In all simulations, the magnetosomes have been considered to have the same effective volume regardless of the bacterial species used. The center-to-center distance between magnetosomes is approximately 60 nm.[58] Consequently, the dipolar interaction is not expected to vary significantly between different species. However, it is important to note that the AMB-1 species does not possess a continuous chain, which may alter this interaction.

Simulated SAR/f values obtained from the area of the simulated hysteresis loops, shown in Figure 5, demonstrate that at low magnetic field strengths, there is no heating response. Above the threshold field, the SAR/f values exhibit a rapid increase due to two factors: the rotation of the magnetization and the orientation of the bacteria in the direction of the magnetic field. As previously stated, in order to account for the rotational factor of the bacteria in the magnetization process, a Gaussian distribution has been introduced that considers the orientation of the bacteria with respect to the applied field. The standard deviation used in each case, σ_α, is shown in Figure 5. It can be observed that, initially, the bacteria are randomly dispersed. Subsequently, above a threshold field they begin to orientate themselves, reaching a high orientation degree for fields where SAR/f saturation takes place. The way the bacteria orient themselves in the direction of the magnetic field depends on the magnetic moment of each bacterium, the amplitude of the magnetic field and the viscosity of the medium, but in this case the rotation is mainly controlled by the high bacterial concentration used in the SAR measurements. The SAR measurements were carried out with a bacterial concentration around 0.5 10^{11} cells/mL for AMB-1 and 10^{11} cells/mL for MSR-1 and MV-1. However, in the case of MV-1, it is important to note that not all individual bacteria possess magnetosome chains. This results in difficulty in orienting the bacteria in the direction of the magnetic field, which in turn leads to a higher final standard angular deviation of the magnetosome chain, σ_α = 30°.

Finally, as the K_{eff} value is increased, the saturated SAR/f values become higher, but at the same time the threshold magnetic field for observing a SAR response increases as well. This is a crucial aspect to consider when selecting a species to be employed as a hyperthermia agent.

CONCLUSIONS

We have carried out a systematic study of the heating efficiency, SAR, of different magnetotactic bacterial species that synthesize magnetosomes with different morphologies and different chain arrangements. The SAR values, measured at a frequency of 132 kHz, were obtained from the area of the AC hysteresis loops. All the species studied show a similar qualitative SAR behavior as a function of the applied field, i.e. the response is very weak at low fields and above a threshold magnetic field, which depends on the species, the SAR increases rapidly until saturation is reached. The values of the effective uniaxial anisotropy of each species were obtained by simulating the AC hysteresis loops using the dynamic Stoner−Wohlfarth model. From the simulations it was observed that as the K_{eff} value increases, there is a corresponding increase in the saturated SAR values. However, the threshold magnetic field required to observe a SAR response becomes larger too.

The findings in this work underscore the importance of considering both magnetic anisotropy and threshold field requirements when selecting a species for use as a hyperthermia agent. The species with the highest magnetic anisotropy is not necessarily the most suitable, as it demands the application of a higher magnetic field to achieve an optimal response. This is critical for researchers working in hyperthermia, as it highlights the need to balance effective anisotropy and field strength to optimize heating efficiency and therapeutic efficacy.

ASSOCIATED CONTENT

Supporting Information

The Supporting Information is available free of charge at https://pubs.acs.org/doi/10.1021/acsami.4c13152.

TEM analysis of bacteria images: Histograms of width (W_m) and length (L_m) of magnetosomes, shape factor parameter (W_m/L_m), cell length (L_{cell}) and magnetosome chain length (L_{mc}) and number of magnetosomes per cell (N_m) for MSR-1, AMB-1 and MV-1 species. Experimental and simulated AC hysteresis loops at

https://doi.org/10.1021/acsami.4c13152
ACS Appl. Mater. Interfaces 2024, 16, 67216−67224

different magnetic field amplitudes at 132 kHz for the MSR-1, AMB-1 and MV-1 species (PDF)

AUTHOR INFORMATION

Corresponding Author

M. Luisa Fdez-Gubieda − *Departamento de Electricidad y Electrónica, Universidad del País Vasco (UPV/EHU), 48940 Leioa, Spain; Basque Center for Materials Applications and Nanostructures (BCMaterials) UPV/EHU Science Park, 48940 Leioa, Spain;* orcid.org/0000-0001-6076-7738; Email: malu.gubieda@ehu.eus

Authors

Danny Villanueva − *Departamento de Electricidad y Electrónica, Universidad del País Vasco (UPV/EHU), 48940 Leioa, Spain;* orcid.org/0000-0001-5700-9442

Alicia G. Gubieda − *Departamento de Inmunología, Microbiología y Parasitología, Universidad del País Vasco (UPV/EHU), 48940 Leioa, Spain;* orcid.org/0000-0002-7598-2008

Lucía Gandarias − *Departamento de Inmunología, Microbiología y Parasitología, Universidad del País Vasco (UPV/EHU), 48940 Leioa, Spain; Institute of Biosciences and Biotechnologies of Aix-Marseille (BIAM), Aix-Marseille Université, CNRS, CEA-UMR 7265, 13108 Saint-Paul-lez-Durance, France;* orcid.org/0000-0001-5749-971X

Ana Abad Díaz de Cerio − *Departamento de Inmunología, Microbiología y Parasitología, Universidad del País Vasco (UPV/EHU), 48940 Leioa, Spain;* orcid.org/0000-0001-6022-1751

Iñaki Orue − *SGIker Medidas Magnéticas, Universidad del País Vasco (UPV/EHU), 48940 Leioa, Spain*

José Ángel García − *Departamento de Física, Universidad del País Vasco (UPV/EHU), 48940 Leioa, Spain*

David de Cos − *Departamento de Física, Universidad del País Vasco (UPV/EHU), 48940 Leioa, Spain*

Javier Alonso − *Departamento CITIMAC, Universidad de Cantabria (UC), 39005 Santander, Spain;* orcid.org/0000-0003-0045-5390

Complete contact information is available at: https://pubs.acs.org/10.1021/acsami.4c13152

Notes

The authors declare no competing financial interest.

ACKNOWLEDGMENTS

This work was supported by the Spanish MCIN/AEI/10.13039/501100011033 under project PID2020-115704RB-C31 and by Spanish MCIU/AEI/10.13039/501100011033/FEDER, UE under project PID2023-146448OB-21 and the Basque Government under projects IT-1479-22 and IT-1800-22. L.G. would like to acknowledge the financial support provided through a postdoctoral fellowship from the Basque Government (POS_2022_1_0017). D.V. gratefully acknowledges grant PRE2021-099247 funded by MCIN/AEI/10.13039/501100011033 and by "ESF Investing in your future". We also thank R. Andrade for technical and human support provided by SGIker (UPV/EHU/FEDER, EU).

REFERENCES

(1) Ferlay, J.; Colombet, M.; Soerjomataram, I.; Parkin, D. M.; Piñeros, M.; Znaor, A.; Bray, F. Cancer Statistics for the Year 2020: An Overview. *Int. J. Cancer* **2021**, *149* (4), 778−789.

(2) Kritika; Roy, I. Therapeutic Applications of Magnetic Nanoparticles: Recent Advances. *Mater. Adv.* **2022**, *3* (20), 7425−7444.

(3) Pankhurst, Q. A.; Connolly, J.; Jones, S. K.; Dobson, J. Applications of Magnetic Nanoparticles in Biomedicine. *J. Phys. D: Appl. Phys.* **2003**, *36* (13), R167−R181.

(4) Yang, M.; Yang, F.; Chen, W.; Liu, S.; Qiu, L.; Chen, J. Bacteria-Mediated Cancer Therapies: Opportunities and Challenges. *Biomater. Sci.* **2021**, *9* (17), 5732−5744.

(5) Duong, M. T. Q.; Qin, Y.; You, S. H.; Min, J. J. Bacteria-Cancer Interactions: Bacteria-Based Cancer Therapy. *Exp. Mol. Med.* **2019**, *51* (12), 1−15.

(6) Zhou, S.; Gravekamp, C.; Bermudes, D.; Liu, K. Tumour-Targeting Bacteria Engineered to Fight Cancer. *Nat. Rev. Cancer* **2018**, *18* (12), 727−743.

(7) Forbes, N. S. Engineering the Perfect (Bacterial) Cancer Therapy. *Nat. Rev. Cancer* **2010**, *10* (11), 785−794.

(8) Lin, D.; Shen, Y.; Liang, T. Oncolytic Virotherapy: Basic Principles, Recent Advances and Future Directions. *Signal Transduction Targeted Ther.* **2023**, *8* (1), 156.

(9) Shalhout, S. Z.; Miller, D. M.; Emerick, K. S.; Kaufman, H. L. Therapy with Oncolytic Viruses: Progress and Challenges. *Nat. Rev. Clin. Oncol.* **2023**, *20* (3), 160−177.

(10) Lal, G.; Rajala, M. S. Recombinant Viruses with Other Anti-Cancer Therapeutics: A Step towards Advancement of Oncolytic Virotherapy. *Cancer Gene Ther.* **2018**, *25* (9−10), 216−226.

(11) Gavilán, H.; Avugadda, S. K.; Fernández-Cabada, T.; Soni, N.; Cassani, M.; Mai, B. T.; Chantrell, R.; Pellegrino, T. Magnetic Nanoparticles and Clusters for Magnetic Hyperthermia: Optimizing Their Heat Performance and Developing Combinatorial Therapies to Tackle Cancer. *Chem. Soc. Rev.* **2021**, *50* (20), 11614−11667.

(12) Lavorato, G. C.; Das, R.; Alonso Masa, J.; Phan, M. H.; Srikanth, H. Hybrid Magnetic Nanoparticles as Efficient Nanoheaters in Biomedical Applications. *Nanoscale Adv.* **2021**, *3* (4), 867−888.

(13) Alphandéry, E.; Chebbi, I.; Guyot, F.; Durand-Dubief, M. Use of Bacterial Magnetosomes in the Magnetic Hyperthermia Treatment of Tumours: A Review. *Int. J. Hyperthermia* **2013**, *29* (8), 801.

(14) Rytov, R. A.; Bautin, V. A.; Usov, N. A. Towards Optimal Thermal Distribution in Magnetic Hyperthermia. *Sci. Rep.* **2022**, *12* (1), 3023−3029.

(15) Thong, P. Q.; Thu Huong, L. T.; Tu, N. D.; My Nhung, H. T.; Khanh, L.; Manh, D. H.; Nam, P. H.; Phuc, N. X.; Alonso, J.; Qiao, J.; Sridhar, S.; Thu, H. P.; Phan, M. H.; Kim Thanh, N. T. Multifunctional Nanocarriers of Fe3O4@PLA-PEG/Curcumin for MRI, Magnetic Hyperthermia and Drug Delivery. *Nanomedicine* **2022**, *17* (22), 1677−1693.

(16) Carter, T. J.; Agliardi, G.; Lin, F. Y.; Ellis, M.; Jones, C.; Robson, M.; Richard-Londt, A.; Southern, P.; Lythgoe, M.; Zaw Thin, M.; Ryzhov, V.; de Rosales, R. T. M.; Gruettner, C.; Abdollah, M. R. A.; Pedley, R. B.; Pankhurst, Q. A.; Kalber, T. L.; Brandner, S.; Quezada, S.; Mulholland, P.; Shevtsov, M.; Chester, K. Potential of Magnetic Hyperthermia to Stimulate Localized Immune Activation. *Small* **2021**, *17* (14), 2005241.

(17) Wang, B.; Qin, Y.; Liu, J.; Zhang, Z.; Li, W.; Pu, G.; Yuanhe, Z.; Gui, X.; Chu, M. Magnetotactic Bacteria-Based Drug-Loaded Micromotors for Highly Efficient Magnetic and Biological Double-Targeted Tumor Therapy. *ACS Appl. Mater. Interfaces* **2023**, *15* (2), 2747−2759.

(18) Chen, C.; Wang, P.; Chen, H.; Wang, X.; Halgamuge, M. N.; Chen, C.; Song, T. Smart Magnetotactic Bacteria Enable the Inhibition of Neuroblastoma under an Alternating Magnetic Field. *ACS Appl. Mater. Interfaces* **2022**, *14* (12), 14049−14058.

(19) Fdez-Gubieda, M. L.; Alonso, J.; García-Prieto, A.; García-Arribas, A.; Fernández Barquín, L.; Muela, A. Magnetotactic Bacteria for Cancer Therapy. *J. Appl. Phys.* **2020**, *128* (7), 070902.

(20) Muela, A.; Muñoz, D.; Martín-Rodríguez, R.; Orue, I.; Garaio, E.; Abad Díaz de Cerio, A.; Alonso, J.; García, J. Á.; Fdez-Gubieda, M. L. Optimal Parameters for Hyperthermia Treatment Using Biomineralized Magnetite Nanoparticles: Theoretical and Experimental Approach. *J. Phys. Chem. C* **2016**, *120* (42), 24437−24448.
(21) Toro-Nahuelpan, M.; Giacomelli, G.; Raschdorf, O.; Borg, S.; Plitzko, J. M.; Bramkamp, M.; Schüler, D.; Müller, F. D. MamY Is a Membrane-Bound Protein That Aligns Magnetosomes and the Motility Axis of Helical Magnetotactic Bacteria. *Nat. Microbiol.* **2019**, *4* (11), 1978−1989.
(22) Blakemore, R. P. Magnetotactic Bacteria. *Annu. Rev. Microbiol.* **1982**, *36*, 217−238.
(23) Uebe, R.; Schüler, D. Magnetosome Biogenesis in Magnetotactic Bacteria. *Nat. Rev. Microbiol.* **2016**, *14* (10), 621−637.
(24) Jogler, C.; Schüler, D. Genomics, Genetics, and Cell Biology of Magnetosome Formation. *Annu. Rev. Microbiol.* **2009**, *63*, 501−521.
(25) Faivre, D.; Schüler, D. Magnetotactic Bacteria and Magnetosomes. *Chem. Rev.* **2008**, *108* (11), 4875−4989.
(26) Bazylinski, D. A.; Frankel, R. B. Magnetosome Formation in Prokaryotes. *Nat. Rev. Microbiol.* **2004**, *2* (3), 217−230.
(27) Gavilán, H.; Simeonidis, K.; Myrovali, E.; Mazarío, E.; Chubykalo-Fesenko, O.; Chantrell, R.; Balcells, L.; Angelakeris, M.; Morales, M. P.; Serantes, D. How Size, Shape and Assembly of Magnetic Nanoparticles Give Rise to Different Hyperthermia Scenarios. *Nanoscale* **2021**, *13* (37), 15631.
(28) Valdés, D. P.; Lima, E.; Zysler, R. D.; Goya, G. F.; De Biasi, E. Role of Anisotropy, Frequency, and Interactions in Magnetic Hyperthermia Applications: Noninteracting Nanoparticles and Linear Chain Arrangements. *Phys. Rev. Appl.* **2021**, *15* (4), 044005.
(29) Nemati, Z.; Alonso, J.; Rodrigo, I.; Das, R.; Garaio, E.; García, J. Á.; Orue, I.; Phan, M. H.; Srikanth, H. Improving the Heating Efficiency of Iron Oxide Nanoparticles by Tuning Their Shape and Size. *J. Phys. Chem. C* **2018**, *122* (4), 2367−2381.
(30) Alphandéry, E.; Faure, S.; Seksek, O.; Guyot, F.; Chebbi, I. Chains of Magnetosomes Extracted from AMB-1 Magnetotactic Bacteria for Application in Alternative Magnetic Field Cancer Therapy. *ACS Nano* **2011**, *5* (8), 6279−6296.
(31) Gandia, D.; Gandarias, L.; Rodrigo, I.; Robles García, J.; Das, R.; Garaio, E.; García, J. Á.; Phan, M.; Srikanth, H.; Orue, I.; Alonso, J.; Muela, A.; Fdez-Gubieda, M. L. Unlocking the Potential of Magnetotactic Bacteria as Magnetic Hyperthermia Agents. *Small* **2019**, *15* (41), 1902626.
(32) Silva, K. T.; Leão, P. E.; Abreu, F.; López, J. A.; Gutarra, M. L.; Farina, M.; Bazylinski, D. A.; Freire, D. M. G.; Lins, U. Optimization of Magnetosome Production and Growth by the Magnetotactic Vibrio Magnetovibrio Blakemorei Strain MV-1 through a Statistics-Based Experimental Design. *Appl. Environ. Microbiol.* **2013**, *79* (8), 2823−2827.
(33) Schüler, D. Genetics and Cell Biology of Magnetosome Formation in Magnetotactic Bacteria. *FEMS Microbiol Rev* **2008**, *32*, 654−672.
(34) Awal, R. P.; Müller, F. D.; Pfeiffer, D.; Monteil, C. L.; Perrière, G.; Lefèvre, C. T.; Schüler, D. Experimental analysis of diverse actin-like proteins from various magnetotactic bacteria by functional expression in Magnetospirillum gryphiswaldense. *mBio* **2023**, *14* (5), No. e0164923.
(35) Gandia, D.; Gandarias, L.; Marcano, L.; Orue, I.; Gil-Cartón, D.; Alonso, J.; García-Arribas, A.; Muela, A.; Fdez-Gubieda, M. L. Elucidating the Role of Shape Anisotropy in Faceted Magnetic Nanoparticles Using Biogenic Magnetosomes as a Model. *Nanoscale* **2020**, *12* (30), 16081−16090.
(36) Pósfai, M.; Kasama, T.; Dunin-Borkowski, R. E. *Characterization of Bacterial Magnetic Nanostructures Using High-Resolution Transmission Electron Microscopy and off-Axis Electron Holography*; Springer: Berlin, Heidelberg, 2006; Vol. 3, pp 197..
(37) Gandia, D.; Marcano, L.; Gandarias, L.; Villanueva, D.; Orue, I.; Abrudan, R. M.; Valencia, S.; Rodrigo, I.; Ángel García, J.; Muela, A.; Fdez-Gubieda, M. L.; Alonso, J. Tuning the Magnetic Response of Magnetospirillum Magneticum by Changing the Culture Medium: A Straightforward Approach to Improve Their Hyperthermia Efficiency. *ACS Appl. Mater. Interfaces* **2023**, *15* (1), 566.
(38) Marcano, L.; Orue, I.; Gandia, D.; Gandarias, L.; Weigand, M.; Abrudan, R. M.; García-Prieto, A.; García-Arribas, A.; Muela, A.; Fdez-Gubieda, M. L.; Valencia, S. Magnetic Anisotropy of Individual Nanomagnets Embedded in Biological Systems Determined by Axi-Asymmetric X-Ray Transmission Microscopy. *ACS Nano* **2022**, *16* (5), 7398−7408.
(39) Bazylinski, D. A.; Frankel, R. B.; Jannasch, H. W. Anaerobic Magnetite Production by a Marine, Magnetotactic Bacterium. *Nature* **1988**, *334* (6182), 518−519.
(40) Saha, P. K.; Borgefors, G.; Sanniti Di Baja, G. Skeletonization and Its Applications − a Review. *Skeletonization: Theory, Methods and Applications*; Academic Press, 2017; pp 3−42..
(41) Rodrigo, I.; Castellanos-Rubio, I.; Garaio, E.; Arriortua, O. K.; Insausti, M.; Orue, I.; García, J. Á.; Plazaola, F. Exploring the Potential of the Dynamic Hysteresis Loops via High Field, High Frequency and Temperature Adjustable AC Magnetometer for Magnetic Hyperthermia Characterization. *Int. J. Hyperthermia* **2020**, *37* (1), 976−991.
(42) Scheffel, A.; Gärdes, A.; Grünberg, K.; Wanner, G.; Schüler, D. The Major Magnetosome Proteins MamGFDC Are Not Essential for Magnetite Biomineralization in Magnetospirillum Gryphiswaldense but Regulate the Size of Magnetosome Crystals. *J. Bacteriol.* **2008**, *190* (1), 377−386.
(43) Murat, D.; Falahati, V.; Bertinetti, L.; Csencsits, R.; Körnig, A.; Downing, K.; Faivre, D.; Komeili, A. The Magnetosome Membrane Protein, MmsF, Is a Major Regulator of Magnetite Biomineralization in Magnetospirillum Magneticum AMB-1. *Mol. Microbiol.* **2012**, *85* (4), 684−699.
(44) Li, J.; Pan, Y.; Chen, G.; Liu, Q.; Tian, L.; Lin, W. Magnetite Magnetosome and Fragmental Chain Formation of Magnetospirillum Magneticum AMB-1: Transmission Electron Microscopy and Magnetic Observations. *Geophys. J. Int.* **2009**, *177*, 33−42.
(45) Thomas-Keprta, K. L.; Bazylinski, D. A.; Kirschvink, J. L.; Clemett, S. J.; McKay, D. S.; Wentworth, S. J.; Vali, H.; Gibson, E. K.; Romanek, C. S. Elongated prismatic magnetite crystals in ALH84001 carbonate globules: *Geochim. Cosmochim. Acta* **2000**, *64* (23), 4049−4081.
(46) Dennis, C. L.; Ivkov, R. Physics of Heat Generation Using Magnetic Nanoparticles for Hyperthermia. *Int. J. Hyperthermia* **2013**, *29* (8), 715−729.
(47) Andreu, I.; Natividad, E. Accuracy of Available Methods for Quantifying the Heat Power Generation of Nanoparticles for Magnetic Hyperthermia. *Int. J. Hyperthermia* **2013**, *29* (8), 739−751.
(48) Martinez-Boubeta, C.; Simeonidis, K.; Makridis, A.; Angelakeris, M.; Iglesias, O.; Guardia, P.; Cabot, A.; Yedra, L.; Estradé, S.; Peiró, F.; Saghi, Z.; Midgley, P. A.; Conde-Leborán, I.; Serantes, D.; Baldomir, D. Learning from Nature to Improve the Heat Generation of Iron-Oxide Nanoparticles for Magnetic Hyperthermia Applications. *Sci. Rep.* **2013**, *3*, 1652−1658.
(49) Nemati, Z.; Alonso, J.; Martinez, L. M.; Khurshid, H.; Garaio, E.; Garcia, J. A.; Phan, M. H.; Srikanth, H. Enhanced Magnetic Hyperthermia in Iron Oxide Nano-Octopods: Size and Anisotropy Effects. *J. Phys. Chem. C* **2016**, *120* (15), 8370−8379.
(50) Khurshid, H.; Alonso, J.; Nemati, Z.; Phan, M. H.; Mukherjee, P.; Fdez-Gubieda, M. L.; Barandiarán, J. M.; Srikanth, H. Anisotropy Effects in Magnetic Hyperthermia: A Comparison between Spherical and Cubic Exchange-Coupled FeO/Fe3O4 Nanoparticles. *J. Appl. Phys.* **2015**, *117* (17), 17A337.
(51) Faílde, D.; Ocampo-Zalvide, V.; Serantes, D.; Iglesias, O. . Understanding Magnetic Hyperthermia Performance within the "Brezovich Criterion": Beyond the Uniaxial Anisotropy Description. *arXiv* **2024**, arXiv:2405.20756.
(52) Carrey, J.; Mehdaoui, B.; Respaud, M. Simple Models for Dynamic Hysteresis Loop Calculations of Magnetic Single-Domain Nanoparticles: Application to Magnetic Hyperthermia Optimization. *J. Appl. Phys.* **2011**, *109* (8), 83921.
(53) Néel, L. Some Theoretical Aspects of Rock-Magnetism. *Adv. Phys.* **1955**, *4* (14), 191.

(54) Vogler, C.; Bruckner, F.; Suess, D.; Dellago, C. Calculating Thermal Stability and Attempt Frequency of Advanced Recording Structures without Free Parameters. *J. Appl. Phys.* **2015**, *117* (16), 163907.
(55) Morales, I.; Costo, R.; Mille, N.; Carrey, J.; Hernando, A.; de la Presa, P. Time-Dependent AC Magnetometry and Chain Formation in Magnetite: The Influence of Particle Size, Initial Temperature and the Shortening of the Relaxation Time by the Applied Field. *Nanoscale Adv.* **2021**, *3* (20), 5801−5812.
(56) Mille, N.; De Masi, D.; Faure, S.; Asensio, J. M.; Chaudret, B.; Carrey, J. Probing Dynamics of Nanoparticle Chains Formation during Magnetic Hyperthermia Using Time-Dependent High-Frequency Hysteresis Loops. *Appl. Phys. Lett.* **2021**, *119* (2), 22407.
(57) Asensio, J. M.; Marbaix, J.; Mille, N.; Lacroix, L. M.; Soulantica, K.; Fazzini, P. F.; Carrey, J.; Chaudret, B. To Heat or Not to Heat: A Study of the Performances of Iron Carbide Nanoparticles in Magnetic Heating. *Nanoscale* **2019**, *11* (12), 5402−5411.
(58) Orue, I.; Marcano, L.; Bender, P.; García-Prieto, A.; Valencia, S.; Mawass, M. A.; Gil-Cartón, D.; Alba Venero, D.; Honecker, D.; García-Arribas, A.; Fernández Barquín, L.; Muela, A.; Fdez-Gubieda, M. L. Configuration of the Magnetosome Chain: A Natural Magnetic Nanoarchitecture. *Nanoscale* **2018**, *10* (16), 7407−7419.

https://doi.org/10.1021/acsami.4c13152
ACS Appl. Mater. Interfaces 2024, 16, 67216−67224